Research Article ISSN 2771-9057

Recent Advances in Clinical Trials

# Fluid–thermal Control of PMMA Cementation for Long Femoral Stems

**Chi-Ming Chiang, MD, PhD[1,2*]**

[1]*Center for General Education, Chung Yuan Christian University, Taoyuan, Taiwan, China.*

[2]*Department of Orthopedics, Yi-Her Hospital, Choninn Medical Group, New Taipei City, Taiwan, China.*

***Correspondence:**

Chi-Ming Chiang, MD, PhD, Center for General Education, Chung Yuan Christian University, Taoyuan, Taiwan, China.

**Received:** 01 Dec 2025; **Accepted:** 25 Dec 2025; **Published:** 17 Jan 2026

**Citation:** Chi-Ming Chiang. Fluid–thermal Control of PMMA Cementation for Long Femoral Stems. Recent Adv Clin Trials. 2026; 6(1): 1-5.

## ABSTRACT

***Background:*** *PMMA cementation couples time-dependent, non-Newtonian flow with exothermic polymerization. Long femoral stems challenge mantle control because viscosity rise, canal pressurization, and insertion kinematics must be coordinated over a larger cement volume while maintaining a conservative thermal window.*

***Methods:*** *We implemented a fluid–thermal control law (μ–Δp–U–δ) emphasizing early low-viscosity continuous pressurization with proximal sealing, an isovelocity stem-insertion trajectory, and δ-guided mantle balancing using surgeon-observable resistance/back-pressure cues. Postoperative radiographs were graded for cement quality (Barrack; Gruen zones) and calibrated mantle thickness, with an a priori target of 2–4 mm.*

***Results:*** *The cement mantle was continuous (Barrack A–B on AP and B on lateral) with no radiolucent lines >1 mm. Calibrated mantle thickness was predominantly within the 2–4 mm target band, with a focal maximum of 7.5 mm; no periprosthetic fracture occurred.*

***Conclusion:*** *Framing cementation as a coupled fluid–thermal control problem provided a practical pathway to achieve a high-quality mantle in a long-stem construct. Thermal risk was constrained by design (pre-cooling, sustained pressure plateau, and avoidance of thick cement pockets) relative to a conservative ≈47 °C × 60 s criterion, motivating prospective validation with intraoperative pressure/temperature logging.*

*Translational potential of this article: A low-dimensional control law—operationally visible to surgeons as timing (μ), steadiness (Δp), and kinematics (U), with δ as a proxy for thickness uniformity—can steer cementation toward a reproducible 2–4 mm mantle even for long stems. The framework is directly testable with intraoperative pressure/temperature logging and bench thermal characterization.*

## Keywords

PMMA bone cement, Cementation, Long femoral stem, Cement mantle thickness, Process control, Pressurization, Thermal safety.

## Introduction

PMMA cementation is a coupled fluid and thermal process: time- and temperature-dependent, shear-thinning rheology drives pressure-assisted interdigitation into cancellous bone, while free-radical polymerization releases heat [1-3]. Contemporary guidance emphasizes modern cementing technique and the geometric importance of a continuous 2–4 mm mantle [4,5]. *In vivo* and *in vitro* measurements show that intramedullary pressure is highly technique dependent and can peak during stem insertion, providing a plausible mechanistic handle for process control via Δp and insertion kinematics [6-9]. We hypothesized that a μ–Δp–U–δ control law can steer the intraoperative process toward a high-quality mantle band—here demonstrated in a long femoral stem—while constraining thermal exposure by design relative to a conservative ≈47 °C × 60 s criterion [10-14].

## Materials and Methods

### Study design and case overview

A modeling-guided clinical case using pre- and postoperative AP radiographs of a cemented long femoral stem in osteopenic morphology. Perioperative steps followed modern cementing practice; the μ–Δp–U–δ schematic and SOP are provided in the Supplementary Material.

### Cementation protocol

Vacuum mixing and retrograde injection were performed after pulse lavage and suction drying [15,16]. A proximal pressurizer maintained a continuous Δp plateau through the low-viscosity window; components and delivery were pre-cooled. The stem was advanced at near-constant velocity without hammering, consistent with evidence that insertion dynamics materially influence intramedullary pressurization [6-9].

### Control framework

Control variables and objectives: μ(t,T,γ̇) denotes the evolving cement viscosity [1-3]; Δp(t) is the intramedullary pressure maintained by proximal sealing and pressurization [6-9]; U is the stem insertion velocity; and δ(t) is a surgeon-observable proxy for mantle non-uniformity, inferred from fluctuations in back-pressure/insertion force and used to guide centering and kinematic adjustments. Radiographically, mantle geometry was quantified by mantle thickness h and focal extrema.

To map a low-dimensional design space, pressure-driven infiltration was represented by a first-order saturation model, $X(t)=X_\infty[1-\exp(-\beta t)]$, where the rate β scales with effective permeability k, pressure Δp, and inverse viscosity μ ($\beta \propto k\Delta p/\mu$). This captures an early-time Darcy-like regime ($X \approx X_\infty \beta t$) and later saturation as available pore space fills. Thermal dose was treated as a design constraint, either by limiting peak temperature (max T<47 °C) or by constraining time above 47 °C ($\int[T-47\ °C]_+ dt \lesssim 60$ s), a conservative threshold often used to operationalize thermal injury risk [14,17-19]. Bench-top thermal/rheological characterization (e.g., DSC-derived kinetics) can provide quantitative priors for μ(t, T) and exotherm modeling [20]. These design constraints map onto standardized acrylic cement descriptors (e.g., doughing time, setting time, and maximum polymerization temperature) as specified in ISO 5833 and ASTM F451, facilitating reproducible benchmarking across cements and laboratories [21,22].

### Radiographic and geometric analyses

Mantle quality was graded (Barrack A–D) and continuity across Gruen zones recorded; radiolucent lines >1 mm were noted [23,24]. Pixel-calibrated mantle thickness was measured at predefined proximal, mid-stem, and distal levels (reported as predominant range and focal extrema); the a priori target was 2–4 mm, with >7 mm pockets flagged. All measurements were performed on the calibrated postoperative AP hip view, acknowledging projection and magnification limitations.

For radiographic calibration, the known implant outer diameter of 50 mm (cup/head) on the postoperative AP hip was used as an in-image scale, yielding a pixel size of approximately 0.515 mm per pixel for that view; all thickness values in (Tables 1,2) were derived using this calibration.

**Table 1:** Calibrated radiographic metrics and calibration parameters.

| Metric | Value | Unit | Notes |
|---|---|---|---|
| Cement mantle thickness (predominant range) | 2–4 | mm | Radiographic target band (calibrated postoperative AP hip view) |
| Cement mantle thickness (focal maximum) | 7.5 | mm | Flag >7 mm pocket |
| Barrack grade (AP/lateral) | A–B / B | — | Continuous across Gruen 1–7 |
| Radiolucent lines (>1 mm) | No | — | |
| In-image calibration object | Cup/head OD = 50 | mm | In-image scale on AP hip view (subject to projection/magnification) |
| Pixel size (AP hip view) | 0.515 | mm/pixel | Derived from 50 mm OD ≈ 97 px |

**Table 2:** Process parameters for the μ–Δp–U–δ control-law (operative SOP).

| Parameter | Target/Setting | Rationale |
|---|---|---|
| μ(t,T,γ̇) | Begin in low-viscosity window | Promote wetting/infiltration |
| Δp | Continuous moderate plateau via proximal pressurizer | Drive pressure-assisted interdigitation; avoid spikes/gaps |
| U | Isovelocity insertion; no hammering | Uniform mantle balancing; reduce periprosthetic fracture risk |
| δ(t) | Back-pressure / insertion-force guided | Surgeon-observable proxy for centering and thickness uniformity |
| Boundary conditions | Pre-cool PMMA & delivery; pulse lavage + suction | Prolong work time; lower peak exotherm; enhance convection |
| Geometry | Maintain 2–4 mm mantle; avoid >7 mm pockets | Constrain thermal dose and improve fatigue/stress behavior |

### Endpoints

Primary endpoints: Barrack A–B continuous mantle predominantly within the 2–4 mm target band; absence of periprosthetic fracture; and thermal conservatism by design referenced to a conservative ≈47 °C × 60 s criterion.

## Results

### Radiographs and mantle geometry

Calibrated mantle thickness was predominantly within 2–4 mm, with a focal maximum thickness of 7.5 mm. The mantle was continuous (Barrack A–B on AP and B on lateral) with no radiolucent lines >1 mm. Representative postoperative radiographs (Figures 1A–C) show a continuous PMMA mantle along the long femoral stem, with radiopaque cement visible distally below the

stem tip, and confirm equal limb length on the long-leg view.


**Figure 1:** Postoperative radiographs of a cemented long femoral stem (de-identified). Panel A (left) shows the AP pelvis for global alignment and limb-length context; prior lumbosacral instrumentation is unrelated to the index procedure. Panel B (right) shows the AP hip demonstrating a continuous PMMA mantle around the long femoral stem (Barrack A–B), central stem position, and no radiolucent lines >1 mm. Panel C shows a long-leg AP radiograph confirming equal limb length and allowing visualization of radiopaque cement along the distal segment below the long stem. The known implant outer diameter (50 mm, cup/head) was used as an in-image calibrator for pixel-to-millimetre conversion.

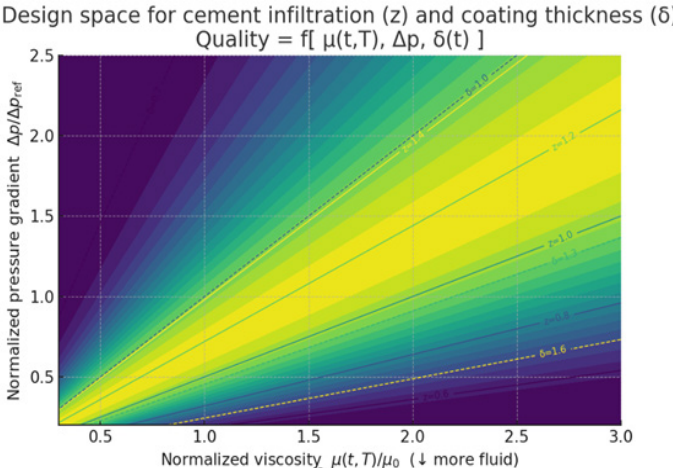


**Figure 2:** μ–Δp design space for cement infiltration (z) and mantle-thickness outcome (h). The diagonal bright band (z≈1.0–1.3; h≈2–4 mm) defines the target operating region. Intraoperatively, δ represents a surgeon-observable proxy used to steer toward this band (e.g., steadiness of resistance/back-pressure reflecting centering and thickness uniformity). Pre-cooling shifts the trajectory left (lower μ); sustained pressurization shifts up (higher Δp); and isovelocity insertion reduces h variance.

## Discussion

In this modeling-guided clinical case, a high-quality cement mantle in a long femoral stem was achieved when cementation was treated as a controlled fluid–thermal process. The key insight is that μ(t, T,γ̇) evolves rapidly during the working phase, and both pressurization strategy and insertion kinematics can exploit the low-μ window to increase penetration while avoiding maldistribution [1-3,6-9]. Experimental studies demonstrate that intramedullary pressure is highly technique dependent and may peak during component insertion rather than during initial compaction, emphasizing the value of maintaining a sustained—but non-spiking—Δp plateau and an isovelocity insertion plan [6-9].

Importantly, the thermal argument in this report is by design rather than by direct measurement: boundary-condition engineering

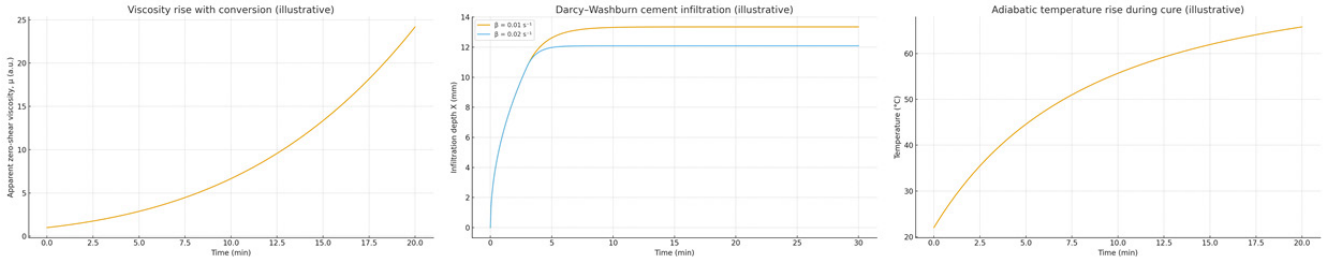


**Figure 3:** Process-level time-courses (a–c): (a) viscosity rise μ(t) identifies the low-μ working window; (b) pressure-driven infiltration represented phenomenologically as X(t)=X∞[1−e^{−βt}] under a steady Δp plateau (β∝kΔp/μ); (c) schematic adiabatic temperature rise motivating the conservative thermal-window rationale (≈47 °C × 60 s).

(pre-cooling, sustained pressurization, avoidance of thick cement pockets) was used to reduce the likelihood of prolonged exposure above a conservative 47 °C threshold, grounded in classic heat-injury experiments [14]. Intraoperative thermocouple studies and computational heat-transfer models provide plausibility for this strategy and clarify why thick cement sections and prolonged setting increase risk [17-19], while DSC-based kinetics can supply quantitative inputs for future model calibration [20].

Limitations include single-case demonstration, reliance on 2D radiographs with in-image calibration, and the absence of intraoperative pressure/temperature traces. Future work should combine intraoperative logging with bench-top rheology/thermal characterization and standardized cement test endpoints (ISO 5833; ASTM F451) to enable reproducible cross-study comparisons [3,20-22], and extend geometric outcomes (e.g., femoral offset) to link process control to functional biomechanics [25-27].

## Conclusions

A μ–Δp–U–δ control-law perspective demonstrated feasibility of achieving a continuous 2–4 mm PMMA mantle in a long-stem construct. The approach is directly translatable as an operative SOP and is suitable for prospective validation with pressure/temperature logging.

## References


1. Ferracane JL, Greener EH. Rheology of acrylic bone cements. Biomater Med Devices Artif Organs. 1981; 9: 213-224.
2. Kolmeder S, Lion A. Characterisation and modelling rheological properties of acrylic bone cement during application. Mech Res Commun. 2013; 48: 93-99.
3. Trivedi Z, Wychowaniec JK, Gehweiler D, et al. Rheological analysis and evaluation of measurement techniques for curing poly(methyl methacrylate) bone cement in vertebroplasty. ACS Biomater Sci Eng. 2024; 10: 4575-4586.
4. Giebel G, Hardt S, Perka C, et al. The cemented stem in hip arthroplasty-state of the art technique and recommendations. EFORT Open Rev. 2024; 9: 1047-1059.
5. Satalich JR, Daniel JL, Simon N, et al. Cementation in total hip arthroplasty: history, principles, and techniques. EFORT Open Rev. 2022; 7: 747-757.
6. Maltry JA, Noble PC, Kamaric E, et al. Factors influencing pressurization of the femoral canal during cemented total hip arthroplasty. J Arthroplasty. 1995; 10: 492-497.
7. Song Y, Goodman SB, Jaffe RA. An in vitro study of femoral intramedullary pressures during hip replacement using modern cement technique. Clin Orthop Relat Res. 1994; 302: 297-304.
8. Churchill DL, Incavo SJ, Uroskie JA, et al. Femoral stem insertion generates high bone cement pressurization. Clin Orthop Relat Res. 2001; 393: 335-344.
9. Bourne RB, Oh I, Harris WH. Femoral cement pressurization during total hip arthroplasty. The role of different femoral stems with reference to stem size and shape. Clin Orthop Relat Res. 1984; 183: 12-16.
10. Szoradi GT, Andrei MF, Sandor GZ, et al. PMMA bone-cement polymerization-induced thermal necrosis-risks and mitigation. Appl Sci. 2024; 14: 11651.
11. Gundapaneni D, Goswami T. Thermal isotherms in PMMA and cell necrosis during total hip arthroplasty. J Appl Biomater Funct Mater. 2014; 12: 193-202.
12. Wang JS, Göran G, Fred K, et al. A modified femoral pressuriser generates a longer-lasting high pressure. J Orthop Surg Res. 2011; 6: 54.
13. Koh BTH, Tan JH, Amit KR, et al. Effect of storage temperature and equilibration time on PMMA handling characteristics. J Orthop Surg Res. 2015; 10: 178.
14. Eriksson AR, Albrektsson T. Temperature threshold levels for heat-induced bone tissue injury: a vital-microscopic study in the rabbit. J Prosthet Dent. 1983; 50: 101-107.
15. Breusch SJ, Norman TL, Schneider U, et al. Lavage technique in total hip arthroplasty: jet lavage produces better cement penetration than syringe lavage in the proximal femur. J Arthroplasty. 2000; 15: 921-927.
16. Wixson RL. Do we need to vacuum mix or centrifuge cement. Clin Orthop Relat Res. 1992; 285: 84-90.
17. Toksvig-Larsen S, Franzen H, Ryd L. Cement interface temperature in hip arthroplasty. Acta Orthop Scand. 1991; 62: 102-105.
18. Swenson LW, Schurman DJ, Piziali RL. Finite element temperature analysis of a total hip replacement and measurement of PMMA curing temperatures. J Biomed Mater Res. 1981; 15: 83-96.
19. Pérez MA, Nuño N, Madrala A, et al. Computational modelling of bone cement polymerization: temperature and residual stresses. Comput Biol Med. 2009; 39: 751-759.
20. Yang JM. Polymerization of acrylic bone cement using differential scanning calorimetry. Biomaterials. 1997; 18: 1293-1298.
21. International Organization for Standardization. ISO 5833:2002. Implants for surgery-Acrylic resin cements. Geneva: ISO; 2002.
22. ASTM International. ASTM F451-21. Standard Specification for Acrylic Bone Cement. West Conshohocken, PA: ASTM International; 2021.
23. Gruen TA, McNeice GM, Amstutz HC. Modes of failure of cemented stem-type femoral components: a radiographic analysis of loosening. Clin Orthop Relat Res. 1979; 17-27.
24. Harvey EJ, Tanzer M, Bobyn JD. Femoral cement grading (Barrack). J Arthroplasty. 1998; 13: 396-401.
25. Rüdiger HA, Maïka G, Adeliya L, et al. Effect of changes of femoral offset on abductor and joint reaction forces in total hip arthroplasty. Arch Orthop Trauma Surg. 2017; 137: 1579-1585.

26. Bahl JS, John BA, David JS, et al. The effect of surgical change to hip geometry on hip biomechanics after primary total hip arthroplasty. J Orthop Res. 2023; 41: 1240-1247.

27. Lecerf G, Fessy MH, Philippot R, et al. Femoral offset: anatomical concept, definition, assessment, implications for preoperative templating and hip arthroplasty. Orthop Traumatol Surg Res. 2009; 95: 210-219.